Hindawi
Journal of Chemistry
Volume 2022, Article ID 5724347, 18 pages
https://doi.org/10.1155/2022/5724347

Research Article

Adsorptive Behavior of Tartaric Acid Treated *Holarrhena antidysenterica* and *Citrullus colocynthis* Biowastes for Decolourization of Congo Red Dye from Aqueous Solutions

Sumaira Basharat,[1] Rabia Rehman ,[1] and Sara Basharat[2]

[1]*Centre for Inorganic Chemistry, School of Chemistry, University of the Punjab, Lahore 54590, Pakistan*
[2]*Institute of Chemistry, University of Education, Lahore, Pakistan*

Correspondence should be addressed to Rabia Rehman; grinorganic@yahoo.com

Received 26 January 2022; Revised 4 April 2022; Accepted 20 April 2022; Published 23 May 2022

Academic Editor: Ana Catarina Sousa

The aim of the present work is to eradicate Congo red (CR) dye from aqueous solutions since the dye compounds are harmful to human life and the environment leading to detrimental results. For this purpose, *Holarrhena antidysenterica* (HA) and *Citrullus colocynthis* (CC) adsorbents were used for the adsorptive removal of Congo red dye from wastewaters. The unmodified adsorbents (U-HA and U-CC) were chemically modified using tartaric acid (TA). Morphological structures were examined by FTIR and SEM. Batch adsorption studies were tested at a variety of pH, time exposure, temperatures, and adsorbent dosages. Thermodynamic parameters such as Gibbs free energy (ΔG°), enthalpy (ΔH°), entropy changes (ΔS°), and energy of activation (E_a) were also calculated. The results revealed that tartaric acid-*Citrullus colocynthis* (TA-CC) gave optimum conditions of time of contact (35 min), temperature conditions (40°C), pH (3), and dosage of adsorbent (1.6 g) for maximum dye removal. Tartaric acid-*Holarrhena antidysenterica* (TA-HA) gave equilibrium time of contact (30 min), temperature (40°C), and pH optimum (2) along with a 1.6 g dosage of adsorbent. Mechanistic understanding of adsorption isotherm provided that the Langmuir model was followed by raw and modified adsorbents. Maximum adsorption capacities Q_{max} attained were 60.61 (mg g^{-1}), 128.21 (mg g^{-1}), 87.71 (mg g^{-1}), and 131.57 (mg g^{-1}), respectively, for U-HA, TA-HA, U-CC, and TA-CC. The results of kinetic modeling displayed a high value of R^2 (0.99) along with minimal error (RMSE) for dye removal showing that the pseudo-second-order kinetic model has acceptable accuracy. Fourier transform infrared proposed the electrostatic, pi-pi interactions, and hydrogen bonding as dominant adsorption mechanisms at acidic pH, respectively. Rate-determining steps comprise both surface and intraparticle diffusions. Thermodynamics indicated that the dye adsorption of CR is spontaneous, exothermic, and favorable in nature. These agricultural wastes due to specific points such as low cost, availability, and high removal rates of adsorption are highly competent for the expulsion of anionic dye like CR from wastewaters.

1. Introduction

Water pollution is a great worry for modern civilization because of industrialization, population sprouts, and urbanization. The last decade has witnessed rapid degradation of the environment and mankind. Metals [1], drugs [2], endocrine disruptor compounds, chiral pesticides [3], paints, plastics, detergents, surfactants, and dyes are directly discharged into the wastewaters. These compounds persist for a longer time and damage ground and surface water esthetics. In humans, these compounds disrupt endocrine functions and affect the normal functionality of the eyes and skin while the sterility of the gonads is affected in male marine animals [4, 5]. Daphnids, sea shrimps, and crayfishes are poisoned [6].

Dyes when released even in minute quantities pose serious threats. They prevent sunlight penetration, retarded growth, and malfunctioning of the aquatic flora and fauna.

Several by-products are released via oxidation and hydrolysis. Their removal has attracted many researchers worldwide empowering a number of technologies for their eradication. These involve chemical procedures (ozonation, oxidation, and ion exchange) [7–9], physical processes (photolysis and magnetic nanocomposites) [10, 11], and biological methods utilizing enzymes and microorganisms [12].

These classical methods are limited to smaller scale, hazardous sludge production, elevated power consumers, costly apparatus and hardware, insufficient removal of ions, and none produce complete removal of colorants from effluents, hence opting for new insights and pathways into this research [13]. Adsorption is favored due to its low cost, simple methodology, high selectivity, environment friendliness, reduced organic solid waste production [14], simple methodology, modest instrumentation, and abundancy of adsorbents [15, 16]. Agricultural biowastes contain carboxyl, carbonyl, amines, and phenolic functional groups that bind cationic and anionic dyes [17] leading towards purified water and valuable components of production.

The world is now shifting towards the manufacturing of smart appliances, such as stimuli-responsive nanoparticles, which control polymer adsorption interactions in colloidal suspension due to electrostatic, steric, and depleting bridged structures. Dye removal was adopted by using photodegradation on nanoparticles. Nanosized photocatalysts are gaining worldwide importance due to extraordinary surface-to-volume proportion [18, 19].

Congo red, an anionic direct diazo dye, is used in paper, printing, leather, and plastic industries. It is also called 3,3′-(biphenyl-4,4′-diyldidiazene-2,1-diyl)bis (4-aminonaphthalene-1-sulfonic acid)) having molecular formula $C_{32}H_{22}N_6Na_2O_6S_2$ and molecular mass of 696.7 g mol^{-1}. Due to its complex aromatic structure (a central biphenyl group along with two symmetric napthalenic groups) [20], it is difficult to degrade from wastewaters, hence posing serious environmental hazards such as eutrophication. In humans, it causes somnolence and eye, skin, and respiratory problems [21]. Lately, CR had been removed by nanocomposite fibres [11], photocatalysis [22], microwave-assisted adsorption [23], advanced oxidation, and adsorption techniques [24].

In the present study, novel biosorbents *Holarrhena antidysenterica* and *Citrullus colocynthis* were used for the elimination of CR from wastewaters. Both of these adsorbents were subjected to tartaric acid modification to enhance the adsorption performances. Since the adsorbents used are waste materials, this experimentation provides positive significance towards solid waste management and valorisation.

The aim of this study is to utilize the aforementioned adsorbents for the sequestration of Congo red from aqueous wastewaters both in raw and tartaric acid-modified forms. The adsorbents were characterized by Fourier Transform Infrared Spectroscopy (FTIR) and scanning electron microscope. Adsorption parameters such as adsorption dosage, pH studies, temperature measurements, and contact times were studied. Thermodynamics, kinetics, and isothermal studies were investigated to elaborate an efficient and comparative research of the batch adsorption process.

2. Experimental Details

2.1. Chemicals and Instrumentation. CR ($C_{32}H_{22}N_6Na_2O_6S_2$, molecular weight = 696.665 g/mol) was utilized as such in contrast to any modification. The adsorbents were collected from local Lahore markets (Pakistan). After washing, sunlight drying, and grinding (60 mesh), the obtained adsorbents were stored in airtight glass containers. Chemical modifications were carried out by soaking adsorbents in a 10% aqueous solution of tartaric acid (Merck). 0.1 M sodium hydroxide (NaOH) (98%, Merck) and 0.1 M hydrochloric acid (HCl) (37%, Merck) solutions were used for pH adjustments. Absorbance was observed at $\lambda_{max} = 498$ nm using UV-Visible Spectrophotometer 720 (China).

Dye solution (1000 mg/L) was prepared by dissolving 1 g of CR/1000 mL distilled water. Further solutions were made by the dilution method. Experiments were performed twice, and average values were calculated. FTIR and SEM analysis were done by Cary 630 Agilent technology (USA) and Nova NanoSem 450 (Thermo Fischer Scientific (USA)).

2.2. Batch Experiments. Experiments were performed in batch mode. Adsorption parameters such as adsorbent dosage, temperature studies, pH, and time of contact were performed using 100 mL CR dye solutions in 250 mL conical flasks. Filtrates were checked for dye concentrations, using a UV-Vis spectrophotometer [25].

Adsorption capacity, q_t (mg·g^{-1}) or amount of CR dye adsorbed on adsorbents at time t, was calculated by following the mass-balance relationship.

$$q_t = (C_o - C_t)\frac{V}{m}, \tag{1}$$

where C_o is the initial CR concentration (mg·L^{-1}), C_t is the dye concentration at any time t, V is the volume of solution (L), and m is the amount of adsorbents used (g). The dye removal efficiency was monitored by

$$\%\text{adsorption} = C_o - \frac{C_t}{C_o} \times 100. \tag{2}$$

3. Results and Discussion

3.1. Chemical Treatment. Chemical pretreatment of biological wastes extracts soluble organic compounds and enhances chelating properties. Different modifying agents such as mineral and organic acids (sulfuric acid, nitric acid, hydrochloric acid, tartaric acid, citric acid, and thioglycolic acid), bases (sodium carbonate, sodium hydroxide, and calcium hydroxide) [26], organic compounds (methanol, formaldehyde, epichlorohydrin, and ethylenediamine), and oxidizing agents (hydrogen peroxide) [27] were used. These entities reduce moisture levels and minimize fungal and bacterial attacks, enhancing adsorbent stability [28]. Uniform distribution of ions increases functionality, and acidic modifications rise protonation [29, 30] and ester linkages [31], exposing more binding sites. Alkali treatment promotes high micropore percentages [32, 33] and swelling and

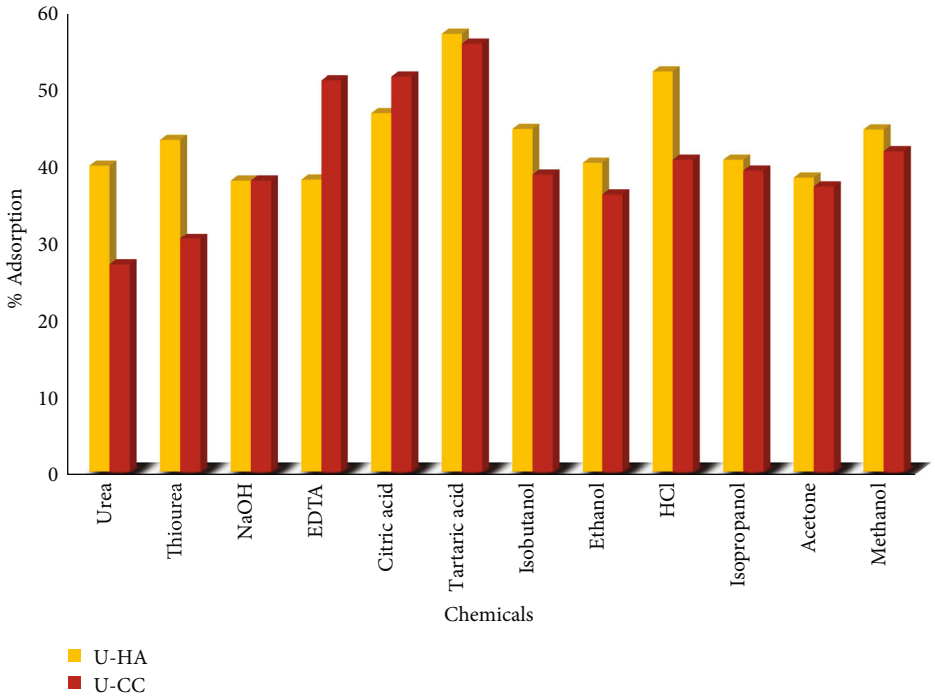

Figure 1: Chemical treatment of adsorbents.

disintegrating of the biomass [34, 35]. Early attainment of equilibrium is achieved [36]. 5 g U-HA and U-CC when dissolved in 25 mL of acidic, basic, and chelating solvents for 4 hours resulted in filtrates that gave the desired results when treated with CR [37]. Tartaric acid gave the most promising results as shown in Figure 1).

3.2. Characterization

3.2.1. Physiochemical Analysis. Physiochemical analysis when performed on the adsorbents gave the following results.

Moisture contents were lesser in CC than in HA. The presence of moisture decreases the pore connectivity and hampers the adsorption process. Bulk, dry densities, and porous nature of CC are nearly the same, slightly elevated than HA. A higher value of particle density, bulk density, and porosity contributes towards greater aesthetics of adsorbents [38, 39]. HA samples bore more ash content components than CC, which can interfere with the pore structure development, leading to increased hydrophilicity and catalytic effects. This causes lower adsorption, decreased mechanical strength, and restricting process during regeneration [40]. Iodine values determine the internal capacity volumes and dispersion degrees of the micropores by determining the amount of iodine adsorbed; thus, the adsorbent capability to eradicate pollutants can be determined. Surface acidity was estimated using Boehm titrations [41]. It was seen that higher acidic groups were present in CC than in HA due to reaction with tartaric acid. Boehm indicated that oxidation groups such as carboxylic acids and phenols were resultant of oxidation reactions. These were present in the lignin, cellulose, and hemicellulose components of the lignocellulosic materials. Overall, *Citrullus colocynthis* (CC) was a better adsorbent than *Holarrhena antidysenterica* (HA) towards the adsorption of CR dye. Table 1 shows the results obtained.

Table 1: Physiochemical properties of adsorbents.

Properties	HA	CC
Bulk density	0.95	0.96
Dry density (g/cm^3)	0.73	0.79
Porosity (%)	0.974	0.975
Moisture (%)	11	07
Ash (%)	23	16
Volatile matter (%)	84.24	76.42
Iodine number (mg/g)	16.92	28.99
Carboxylic groups (mmol)	1.98	1.94
Phenols (mmol)	0.94	0.96
Lactones (mmol)	0.84	1.08

3.2.2. Fourier Transform Infrared Studies (FTIR). Functional groups, organic moieties, and nature of interactions between the dye and adsorbents can be estimated by using FTIR spectroscopy. Figure 2 shows FTIR band frequencies in the span of 400-4000 cm^{-1} for U-HA, TA-HA, U-CC, and TA-CC with CR dye.

U-HA reacts with CR (Figure 2(a)) to give wide stretches at 3737.6 cm^{-1} and 3653.0 cm^{-1} corresponding towards –OH groups of alcohols and phenols, and the peaks at 2922 cm^{-1}, 2918 cm^{-1}, 2853 cm^{-1}, and 2850 cm^{-1} are indicative of asymmetric and symmetric sp^3 C-H stretch [42], while weak peaks of 2371 cm^{-1} show the alkyne or nitrile group. Some peaks of 1654 cm^{-1}, 1636 cm^{-1}, and 1647 cm^{-1} demonstrate aromatic -C=O and C=C linkages of carboxylic acid

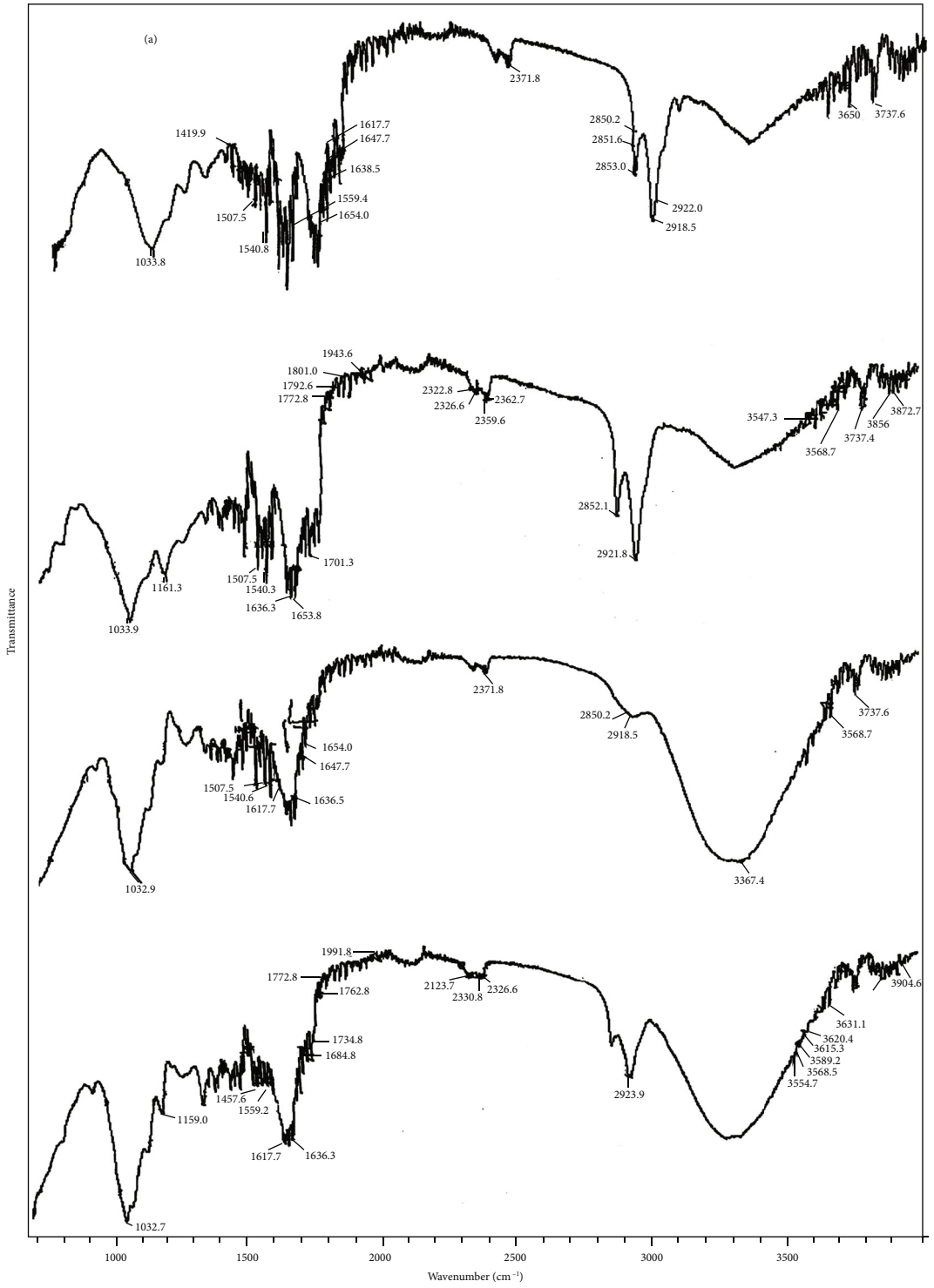

Figure 2: FTIR of raw and modified adsorbents: (a) U-HA-CR, (b) TA-HA-CR, (c) U-CC-CR, and (d) TA-CC-CR.

anions/amide linkages formed between CR and U-HA. When TA-HA was treated with CR (Figure 2(b)), a few additional peaks were observed such as 3872 cm^{-1}, 3856 cm^{-1}, 3737 cm^{-1}, 3568 cm^{-1}, and 3547 cm^{-1} displaying peaks of hydroxyl of alcohols and phenols. Reduced peaks of 2921 cm^{-1} and 2852 cm^{-1} are evident of asymmetrical and symmetrical alkane sp^3 C-H stretch. Weak peaks of 2366 cm^{-1} contribute to alkyne/nitrile moieties. Peaks of 1801 cm^{-1}, 1792 cm^{-1},1772 cm^{-1}, and 1701 cm^{-1} represent C=O peaks of anhydride, carboxylic acids, and aldehydes. Strong peaks at 1653 cm^{-1} and 1636 cm^{-1} are evident of aromatic amides/-C=O/C=C bonds in carboxylic acid anions, indicating the reaction of CR with tartaric acid-treated adsorbent. 1540 cm^{-1} and 1457 cm^{-1} display C-H bending/

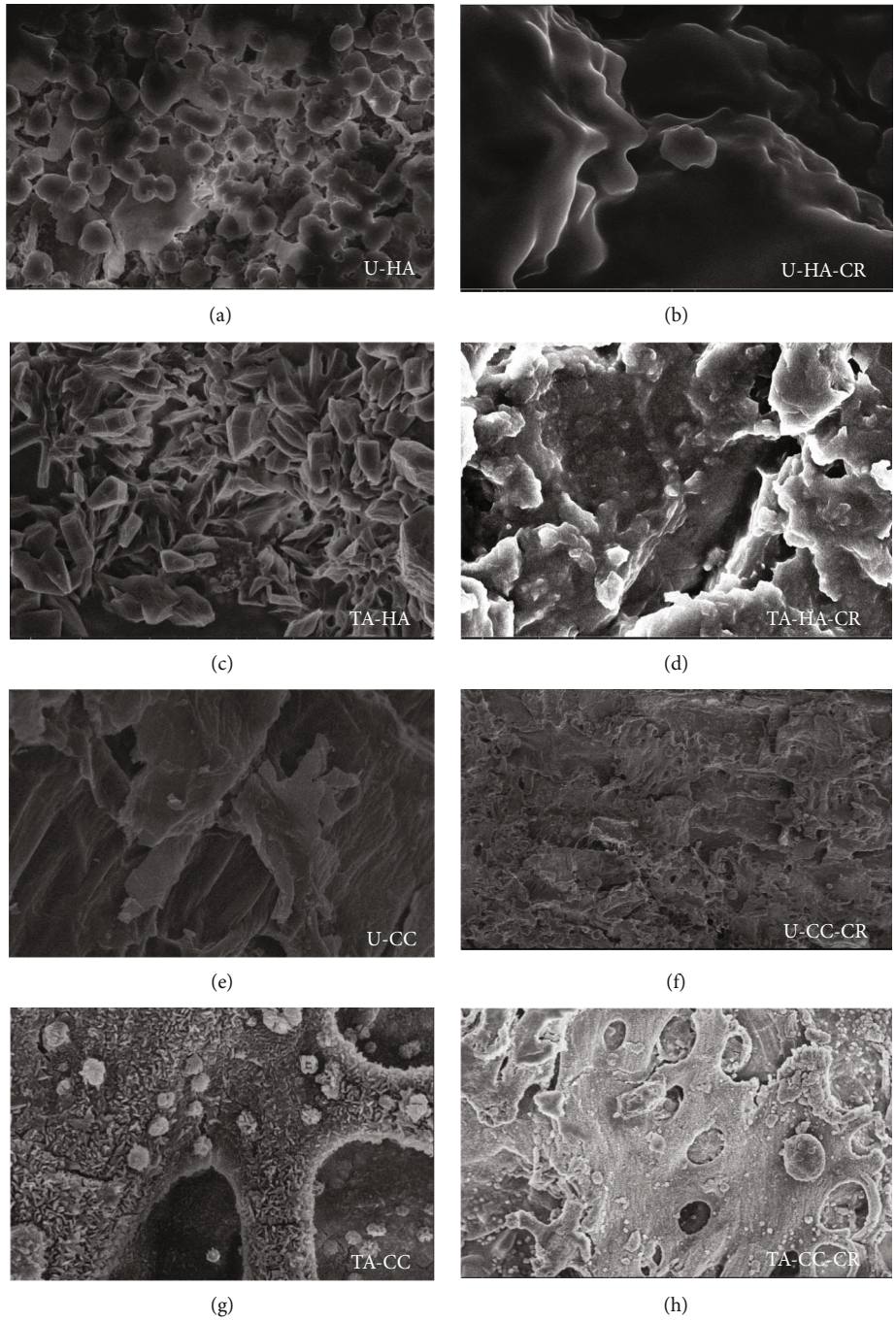

Figure 3: SEM illustrations of (a) U-HA, (b) U-HA-CR, (c) TA-HA, (d) TA-HA-CR, (e) U-CC, (f) U-CC-CR, (g) TA-CC, and (h) TA-CC-CR.

C=C/phenolic OH and –C=O of carboxylates. 1161 cm^{-1} show –C-O of ester linkages formed between tartaric acid and lignocellulosic materials.

The second adsorbent U-CC (Figure 2(c)) when reacted with CR was seen to consist of -OH stretch at 3568 cm^{-1} and 3737 cm^{-1} while alkenyl stretch at 3367 cm^{-1} and alkane C-H at 2850 cm^{-1}. Peaks at 1654 cm^{-1}, 1647 cm^{-1}, and 1636 cm^{-1} display -C=O of amide, aromatic -C=O, and C=C of carboxylic acid anions whereas 1559 cm^{-1} show C-H bending/C=C stretches. When TA-CC was treated with CR (Figure 2(d)), new peaks displaying hydroxyl groups were observed such as 3904 cm^{-1}, 3841 cm^{-1}, 3631 cm^{-1}, and 3547 cm^{-1}. Alkyl C-H stretch was seen at 2923.9 cm^{-1} while 2326 cm^{-1} displayed weak nitrile groups. Weak peaks at 1772 cm^{-1} represent C=O of carboxylic acids, and 1734 cm^{-1} are evident of ester linkages ($–COO^-$)/(–COOR) formed between cellulose and tartaric acids. 1684 cm^{-1} represent amide groups of CR reaction with adsorbent while 1457 cm^{-1} show C-H bend. A strong 1159 cm^{-1} peak is evident of esters.

3.2.3. Scanning Electron Microscopy. SEM was used to investigate the structural properties of raw and modified forms of

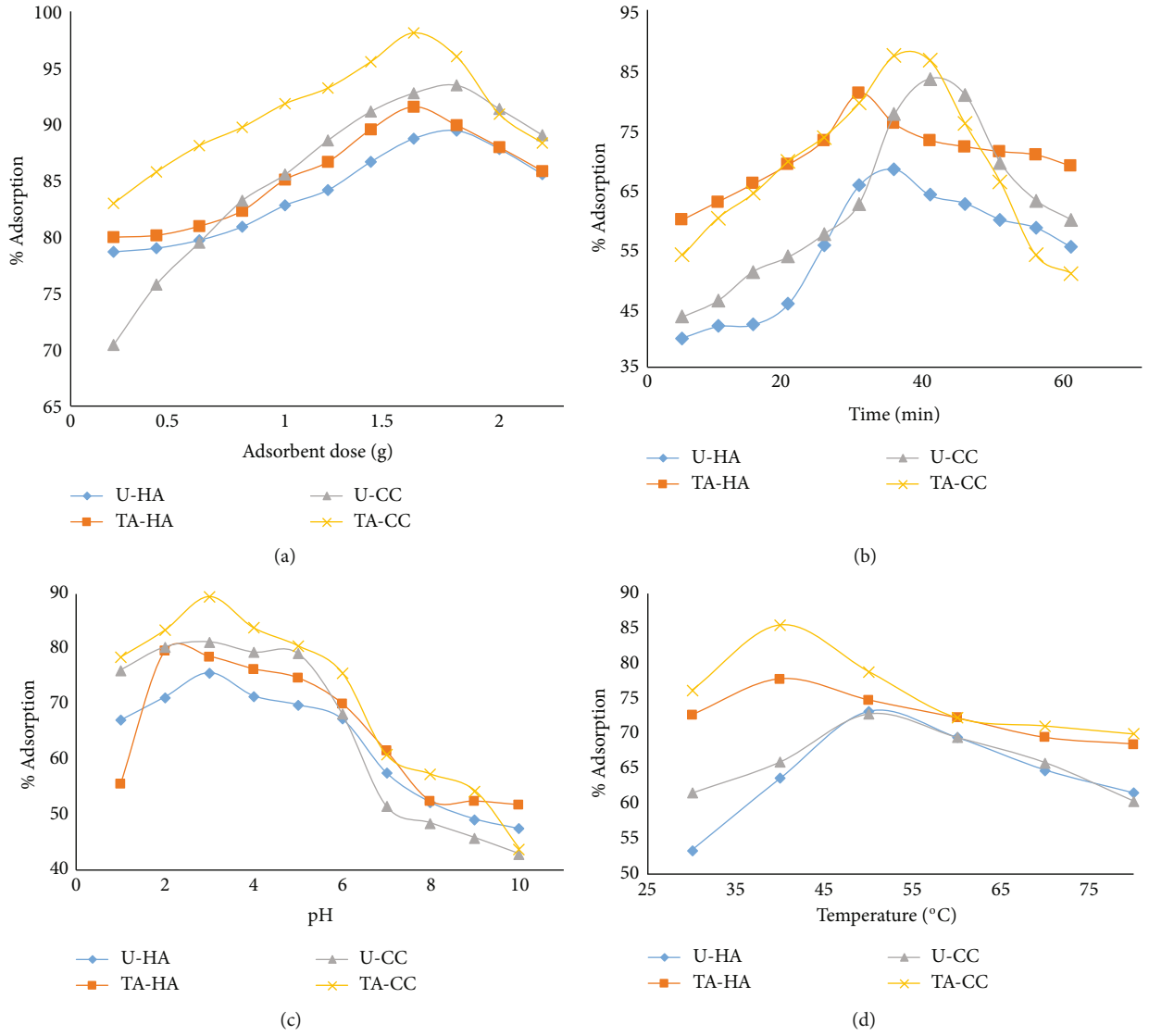

Figure 4: (a) Dosage of adsorbents, (b) contact times, (c) pH changes, and (d) temperature studies for CR eradiation.

adsorbents. It was seen that U-HA consists of porous, irregular, and spherical aggregates (Figure 3(a)) that convert to sharply chiseled structures upon chemical modifications (Figure 3(c)) while the U-CC consists of porous, aggregated plate-shaped structure (Figure 3(e)) that convert towards agglomerated, porous, irregular-shaped structure upon modifications (Figure 3(h)). The tissues are arranged in layers that provide additional adsorbent sites for the sequestration of the dye [43]. When CR was adsorbed, characteristic changes of the phase were observed. Irregular structures were converted to smooth pattern due to the binding of CR dye molecule over the adsorbent sites after CR adsorption (Figures 3(b), 3(d), 3(e), and 3(h))) [39].

3.3. Effect of Adsorbent Dosage. Chemical modification increased the availability of potential sites at lower concentrations; however, overlapping of sites was observed in higher amounts. U-HA removed CR dye up to 89%, and U-CC sequestered 93%, at 1.8 g, whereas TA-HA and TA-CC eradicated 91% and 98% at 1.6 g, respectively (Figure 4 (a)). After reaching maximum adsorption efficiency (91-98%), an increase in dosage does not have much dye sequestration efficiency. This is due to the gradient distribution and active site saturation between the adsorbent and dye [43, 44]. Hence, 1.8 g adsorbent dose for TA-HA and 1.6 g of TA-CC were selected for further experiments as higher concentrations did not yield significant results.

3.4. Effect of Contact Time. The effect of contact time is one of the most important parameters as adsorption mechanism and rate-determining steps are dependent upon its findings [45]. CR dye sequestration by adsorbents is determined by investigating the least time required for achieving equilibrium of dye with the adsorbent. The procedure was carried out for sixty minutes with five minutes time interval until equilibrium was achieved. Adsorption increased at initial stages [46] and decreased at later terminals, where repulsion of adsorbed-non-adsorbed species rendered its efficiency. About 68% CR dye was adsorbed at 35 minutes for U-HA that increased up to 81% at 30 minutes for TA-HA. U-CC

removed 83% of CR at 40 minutes, which rose to 87% at 35 minutes for TA-CC (Figure 4(b)).

3.5. Influence of pH on CR Adsorption. The binding of dye molecules with the adsorbent surface is monitored by pH as it changes the degree of ionization of adsorbed species and properties of adsorbent surfaces [47, 48]. Acidic pH promotes protonation of carboxylic acids, which are present in lignocellulosic materials resulting in acidic adsorption sites. Excess of H^+ ions battles against the positive groups of basic dyes for adsorption surfaces, resulting in repulsion among the cationic groups of adsorbent and dye. A decrease in hydrogen bonding is observed and anionic dye adsorption is favored. Whereas basic pH causes deprotonation of functional moieties, more hydroxyl ions render adsorption of anionic dyes, and positive charges are reduced at solid-liquid interphase, making the adsorption surface negatively charged, attracting cationic colorants. A range of 1-10 pH was selected for the sequestration of the acidic dye. CR dye adsorption depends upon charge and surface characteristics. Point of zero charge (pHpzc) [49, 50] was found to be 5 for U-HA and 6 for U-CC, determined by the electrochemical method [51] in our previous studies [37]. At pH > pHpzc, the adsorbent is negatively charged while it is positive at pH < pHpzc. At lower pH, Congo red is dissociated into polar groups ($R\text{-}SO_3^-$) and the positive surface of adsorbent attracts the sulfonate moieties through electrostatic attractions. While at alkaline pH, higher (OH^-) and (COO^-) concentrations compete with the dye anions for potential sites, offering repulsion and decrease in adsorption capacity [52, 53]. At pH 3, U-HA removed 75% CR which increased to 79% at pH 2 for the treated form. U-CC adsorbed CR up to 81% for untreated adsorbent and 89% for modified forms at pH 3 (Figure 4(c)).

3.6. Temperature. Rise in temperature promotes entropy changes and inflammations in dye particles. An increase in kinetic energy favors the intraparticle diffusion model. The effect of temperature (in the range of 30-80°C) on CR adsorption was studied. 73% adsorption was observed at 50°C for U-HA that rose to 75% at 40°C for modified forms. U-CC was seen to remove 72% at 50°C and 85% for treated adsorbents at 40°C (Figure 4(d)). Removal efficiency decreased after saturation point indicating the reaction to be an exothermic one. Increased mobility of larger dye ion with temperature increases adsorption.

3.7. Kinetic Studies. Rate estimation and mechanistic understanding of adsorption procedure require the performance of kinetic studies. These studies are dependent upon physical and chemical properties of adsorbents and affect the adsorption mechanism [54, 55]. Popular models such as pseudo-first-order, pseudo-second-order [55], and Elovich models [56–58] were considered to elucidate CR adsorption mechanism on adsorbents.

Pseudo-first-order reaction displays dependency of adsorption on freely bounded surfaces. Its linear (Equation (3)) and nonlinear forms (Equation (4)) are shown as follows:

$$\ln\,(q_e - q_t) = \ln\, q_e - k_1 t, \tag{3}$$

$$q_t = q_e(1 - \exp - k_1 t), \tag{4}$$

where q_e (mgg^{-1}) and q_t (mgg^{-1}) are the amounts of CR adsorbed at equilibrium and time t, k_1 (min^{-1}) represents the rate constant for pseudo-first-order reaction. A graph between $\ln\,(q_e - q_t)$ against t yields a straight line, from which k_1 and regression coefficient R^2 are calculated [59].

Reaction kinetics can also be explained by using pseudo-second-order reaction. Linear (Equation (5)) and nonlinear (Equation (6)) forms are as follows:

$$\frac{t}{q_t} = \frac{1}{K_2 q_e^2} + \frac{t}{q_e}, \tag{5}$$

$$q_t = \frac{t.k_2(q_e)^2}{1 + tk_2.q_e}. \tag{6}$$

A plot of t/q_t against t gives k_2 ($g{\cdot}mg^{-1}\,min^{-1}$) which is the equilibrium rate constant. Initial rate of adsorption h ($mg{\cdot}g^{-1}\,min^{-1}$) is given by Equation (7) [46]:

$$h = K_2 q_e^2. \tag{7}$$

The Elovich equation determines the adsorption on heterogeneous adsorbent surfaces. It is represented as linear (Equation (8)) and nonlinear (Equation (9)) as follows:

$$q_t = \frac{\ln\,(\alpha \times \beta)}{\beta} + \frac{\ln\, t}{\beta}, \tag{8}$$

$$q_t = q_e(1 - \exp - k_1 t), \tag{9}$$

where α (mg·min/g) and β (g/mg) are initial process rate constant and factors related to the activation energy for chemical adsorption. A plot between q_t and $\ln t$ gives a straight line from which α and β can be obtained.

Quantitative checking is performed by utilizing percent relative deviation (P) as shown in

$$P = \frac{100}{N} \sum \left\{ \frac{q_{e(\exp)} - q_{e(\mathrm{cal})}}{q_{e(\exp)}} \right\}. \tag{10}$$

Here, $q_{e(\exp)}$ ($mg{\cdot}g^{-1}$) is the experimental adsorption capacities, $q_{e(\mathrm{cal})}$ (mg/g) calculated adsorption capacities, and N represents the total number of observations made during the adsorption experiment. A lower P value is indicative of higher appropriateness of the kinetic data [60].

Absorbance values were demonstrated using 25 mg/L of CR dye solutions at 298 K with a 5-minute interval for retention kinetics. The upper buoyant floating layer of CR was observed. It displayed rapid adsorption in the initial stages that gradually receded as the experiment approached equilibrium.

CR retention on adsorbents (raw and modified) was performed (Table 2). Comparison of correlation coefficient R^2 proves that Ho's model agrees with the experimental data in all states. Moreover, $(q_{e(\mathrm{calc})})$ is in complete agreement to that of $(q_{e(\exp)})$. A smaller variance "P" is observed among

Table 2: Kinetic parameters for CR dye adsorption.

Kinetic models	U-HA	TA-HA	U-CC	TA-CC
Elovich				
a ($g\,mg^{-1}\,min^{-1}$)	2.67	2.43	3.03	4.41
b ($g\,mg^{-1}$)	9.62	4.26	18.05	55.56
R^2	0.9465	0.8752	0.8206	0.5199
RMSE values	0.199637	0.090748	0.286502	0.4375
Pseudo-First order Kinetics				
$q_{e(\text{experimental})}$ ($mg\,g^{-1}$)	1.39	1.56	1.33	1.56
$q_{e(\text{calculated})}$ ($mg\,g^{-1}$)	0.03	0.01	0.02	0.07
k_1 (1/min)	0.19	0.23	0.16	0.21
R^2	0.3724	0.7802	0.8194	0.8413
P	13.67	15.59	13.19	15.09
RMSE	0.37862719	0.43454551	0.38183609	0.45346783
Pseudo-second Order Kinetics				
$1/q$	0.7234	0.6636	0.7443	0.6408
k_2 (g/(mgmin))	0.84	6.52	1.00	2.97
q_e ($mg\,g^{-1}$)	1.38	1.51	1.34	1.56
$t^{1/2}$	0.86	0.10	0.74	0.22
h (mg/g·min)	1.62	14.81	1.81	7.25
R^2	0.9978	0.9991	0.9995	0.9999
P	3.93	5.94	3.26	5.55
RMSE	0.018268723	0.018746589	0.000763183	0.002285479
Intraparticle diffusion				
k_{id} ($mg/(g\,min^{1/2})$)	0.0398	0.0427	0.0265	0.0276
C ($mg\,g^{-1}$)	1.1041	1.279	1.1485	1.4108
R^2	0.891	0.7905	0.7958	0.8904
Film diffusion				
K_{fd} (1/min)	0.0996	0.1298	0.0576	0.0751
R^2	0.958	0.898	0.9093	0.9647

the calculated and experimental values of pseudo-second-order kinetics. An increase in initial adsorption rate "h" and a decline in $t^{1/2}$ were seen as the adsorbents shifted towards the chemically modified structures [32, 61]. Chemisorption at available adsorption sites [62] may be involved in the dye elimination utilizing covalent bonding (sharing or electron transfer) among CR and adsorbents [43, 63]. The Elovich model displayed a least fitting R^2.

3.8. Calculation of Errors. RMSE (Root Mean Square Error) (Equation (11)) was calculated in this study to estimate the deviation among the experimental and calculated observations. The model with the minimum error was the one accepted (Table 2).

$$\text{RMSE} = \sqrt{\sum \frac{\left(q_{e(\text{cal})} - q_{e(\text{exp})}\right)^2}{N}}. \tag{11}$$

Here, $q_{e(\text{exp})}$ (mg/g) defines experimental values, $q_{e(\text{cal})}$ (mg/g) calculated numbers at time t, and N displays total number of observations. The pseudo-second-order model and Langmuir isotherms displayed the least error [64].

3.9. Mass Transfer Parameters. The intraparticle or boundary layer diffusion mechanism is responsible for CR adsorption on raw and treated adsorbents. The complete adsorption procedure consists of multiple steps such as (a) film diffusion, adsorbate heading for the massed adsorbent, (b) intraparticle/pore diffusion, penetration occurs from exterior to interior orifices, and (c) complex forming within the colorant and chemical groups in the adsorbent [65]. The intraparticle diffusion model was popularized for the understanding of the mechanism involved [66]. The Webber and Morris equation is as under

$$q_t = k_{id} t^{1/2}. \tag{12}$$

Here, q_t (mg/g) is the amount adsorbed at time t and k_{id} ($mg\,g^{-1}\,min^{-1/2}$) is the coefficient of intraparticle diffusion. This mechanism is the sole process if the origin is intersected when q_t is plotted against $t^{1/2}$. Multilinear plots show a

variety of steps involved. Initial steps involve adsorbate diffusion on the exterior of the adsorbent or the boundary layer diffusion of solute particles, next is the gradual adsorption phase where the intraparticle diffusion rate becomes limiting. At the last equilibrium stage, intraparticle diffusion slows down due to the least availability of dye particles in the solution [67]. "C" values determine the thickness of the adsorbent layer [44]. When $C = 0$, adsorption is limited and intraparticle diffusion mechanism is involved. Negative C shows an increase in the border layer while positive values are representative of rapid adsorption [68]. The values are raised for the modified forms leading towards the complexity of the adsorption procedure. Table 2 represents the entire figures of the model.

The rate of uptake is limited by the adsorbate's size, diffusion coefficient, concentration, and attraction towards the adsorbent. Degree of mixing, bulk phase, and pore-size distribution of the adsorbent also play an important role. Systems with higher concentrations of dyes, great mixing, higher particle size, and a lower adsorbent affinity towards the adsorbent favor the intraparticle diffusion mechanism [69]. The results are displayed in Figures 5(d) and 5(e).

Boyd's plots involve fractional attainment of equilibrium with time variations [70]:

$$\ln (1 - F) = -\left(K_{fd} t\right), \tag{13}$$

$$F = \frac{q_t}{q_e}. \tag{14}$$

When the graph plotted among B_b and t passes through the origin, the Webber-Morris mechanism is involved. However, if not crossed, the boundary layer/chemical reaction is involved. Figures 5(f) and 5(g) indicate that the mechanism is the boundary layer. Straight paths are following the curved ones with varied adsorption lengths in the initial and final stages. Hence, the boundary layer diffusion prevails in the initial stages while intraparticle in the later ones. Increased K_{fd} values along with higher correlations R^2 against intraparticle (Table 2) are in complete agreement with the proposed mechanism.

3.10. Isothermal Studies. Isothermal study determines the adsorbent's capacity, surface characteristics, and the mechanism of the adsorption process [71]. It was done by selecting 10 mg/L, 15 mg/L, 20 mg/L, 25 mg/L, 30 mg/L, 35 mg/L, and 40 mg/L concentrations of CR dye in 250 mL sealed flasks. Optimum conditions of contact time, temperature, pH, and dose of adsorbent were selected for this study. The equilibrium dye retention was investigated using the Langmuir, Freundlich, Temkin, and Dubnin Radoshkevich (D-R) isotherms.

Langmuir isotherm addresses the adsorption process as monolayered, homogeneously distributed over a fixed number of adsorption sites, involving no interaction among the adsorbed species. Homogeneity is further used for the description of binary system behavior [72].

The linear [73] and nonlinear forms [74] are given as follows:

$$\frac{1}{q_e} = \frac{1}{q_m} + \frac{1}{K_L q_m C_e}, \tag{15}$$

$$q_e = \frac{K_L q_m c_e}{1 + K_L c_e}, \tag{16}$$

where K_L (L/mg) is called the Langmuir constant; q_m (mg/g) is the maximum uptake ability of the adsorbent; C_e (mg/L) is the equilibrium CR dye adsorption. The graph between $1/C_e$ against $1/q_e$ gives the desired plot [75].

Separation factor R_L calculated from Langmuir constants holds prime importance [70]:

$$R_L = \frac{1}{1 + K_L C_o}, \tag{17}$$

where C_o (mg/g) is the initial CR concentration. The adsorption process is unfavorable if $R_L > 1$, linear if $R_L = 1$, appropriate if $0 < R_L < 1$, and irreversible if $R_L = 0$.

Freundlich isotherms is another model used for heterogeneous, multilayer adsorption systems. This isotherm favors physisorption. Linear (Equation (18)) and nonlinear forms (Equation (19)) of the Freundlich equation are shown as

$$\log q_e = \log K_f + \frac{1}{n} \log C_e, \tag{18}$$

$$q_e = K_f C_e^{\,1/n}, \tag{19}$$

where C_e (mg/L) is the CR dye equilibrium concentrations and q_e (mg/g) is the amount of CR dye adsorbed. k_ff ((mg/g /$(\mathrm{L/mg})^{1/n}$) is the binding constant, and n (g/L) is the adsorption strength. These are determined from the slope and intercept of the straight line when log q_e is plotted against log C_e. Varied adsorption systems (chemical, physical, and linear) are predicted by values of n (heterogeneity factor) [56, 72]. It depends upon the coordination number of dye, dye-adsorbate attractions, Avogadro's number, and Boltzmann constant. A value close to 0 indicates physisorption while near to 1 is imminent of chemical adsorption or cooperative adsorption.

The Temkin isotherm demonstrates linear reduction of adsorption heat in all surface structures during adsorbent-dye interactions [76]. Linear (Equation (20)) and nonlinear (Equation (21)) Temkin isotherm is given as

$$q_e = B \ln C_e + B \ln A, \tag{20}$$

$$q_t = \frac{1}{b} (\ln (a.b.t)), \tag{21}$$

where A_T (L/g) is the equilibrium binding constant and B_T ($\mathrm{J{\cdot}mol^{-1}}$) is the heat of adsorption. These are determined

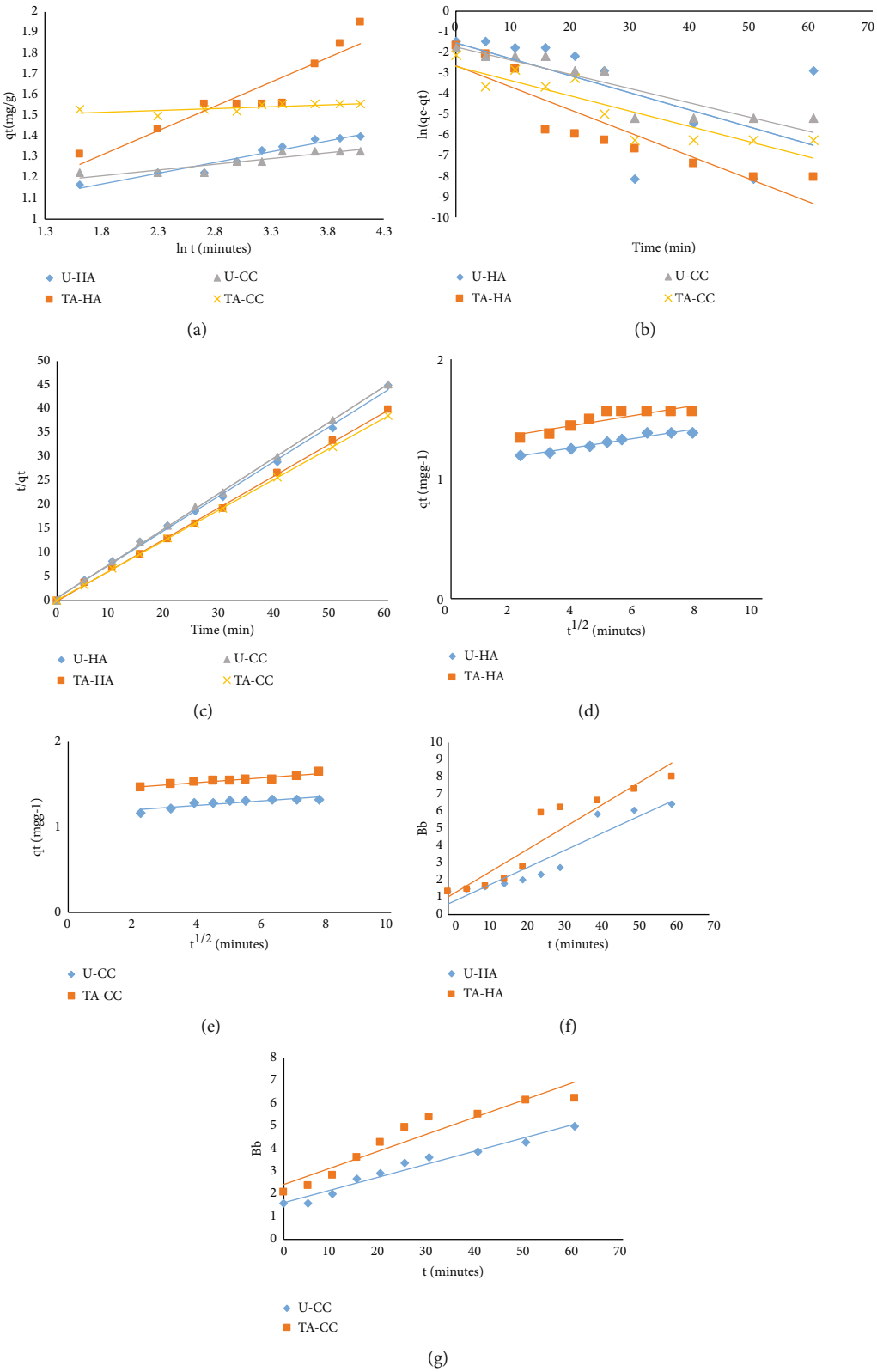

Figure 5: (a) Elovich designs, (b) Pseudo-First-Order kinetics, (c) Pseudo-Second-Order kinetics, (d) Webber-Morris plots (U-HA and TA-HA), (e) Webber-Morris plots (U-CC and TA-CC), (f) Boyd's plots (U-HA and TA-HA), and (g) Boyd's plots (U-CC and TA-CC) for CR dye.

from slope and intercept of linear plots of q_e against ln C_e. B_T lower values than 8 describe weak physical adsorption but higher than 8 correspond to strong chemical adsorption [77, 78]. Moreover, a higher B_T is responsible for rapidity of the rate of adsorption at initial stages while a low A_T ratio is indicative of weak bonds among adsorbent and adsorbate.

Another adsorption isotherm is the Dubnin-Radoshkevich (D-R) isotherm, which considers adsorption on homo- and heterogeneous potential sites [79] for intermediate ranges of concentrations. Complete free energy as well as physical and chemical properties of the procedure is represented in this isotherm. Linear (Equation (22)) and nonlinear form (Equation (24)) of D-R isotherm is given as

$$\ln q_e = \ln q_m - \beta\varepsilon^2, \tag{22}$$

$$\varepsilon = RT \ln\left(1 + \frac{1}{C_e}\right), \tag{23}$$

$$q_e = q_m \exp\left(-\beta\varepsilon^2\right). \tag{24}$$

Using "β" (mol^2/J^2), mean free energy "E" (Equation (25)) is calculated:

$$E = \frac{1}{\sqrt{2\beta}}. \tag{25}$$

The adsorption process depends upon E values, where <8 kJmol^{-1} represents physical adsorption, intermediate range 8-16 kJmol^{-1} shows ion-exchange phenomenon, and >16 kJmol^{-1} shows chemical adsorption process. Plots of ln q_e and $\mathcal{E}^2$ provide linear plots of D-R isotherms [70].

Equilibrium isotherms are used for describing surface characterization and equilibrium behavior between dye and adsorbent (Table 3 and Figure 6). As seen from the table, correlation coefficient R^2 for Langmuir isotherm is in close proximity to one and higher than correlation coefficients of all other isothermic models. Hence, the Langmuir model is more in acceptance towards the experimental data. Q_m for U-CC and its modified forms is higher than U-HA and its treated forms, indicating better CR dye quenching. Hence, adsorption of CR on raw and modified adsorbents is single-layered, homogeneous, and chemically adsorbed process with no side reactions occurring among the molecules [80]. R_L values were lower than one implying a favorable adsorption [71]. Moreover, b values were in favor of CR adsorption on raw and modified adsorbents.

The correlation coefficient of Freundlich, which is lesser, does not favor the physisorption mechanism. Temkin and D-R isotherm lower R^2 values also render fitting of these models towards the experimental values. A higher ratio of potential sites and better chelating abilities of CR are responsible for this trend.

3.11. Thermodynamic Studies. To study the effect of temperature on CR adsorption, temperature-controlled studies were done in the 283 K-323 K range. Equations (26)–(28) were employed for the calculations and represented in (Table 4) along with (Figure 7).

Table 3: Isothermal parameters for CR dye adsorption.

Isotherm models	U-HA	TA-HA	U-CC	TA-CC
Langmuir				
Q_m (mg/g)	60.61	128.21	87.71	131.57
R_L (L mg^{-1})	0.47-0.25	0.12-0.05	0.29-0.13	0.15-0.06
b (L g^{-1})	0.03	0.23	0.07	0.25
R^2	0.9801	0.9812	0.9921	0.9918
RMSE	10.851	3.005	9.4962	1.605805728
Freundlich				
n	0.691	1.53	0.75	1.43
K_f (mg/g)	1.25	25.28	6.32	29.26
R^2	0.9667	0.9672	0.9897	0.9838
RMSE	11.048	3.745	9.924	2.561
Temkin				
B (J mol^{-1})	0.07	0.09	0.07	0.07
A (L g^{-1})	0.25	2.30	0.73	2.03
R^2	0.918186	0.9525	0.9517	0.98
RMSE	14.095	52.701	17.092	25.997
D-R				
Q_m (mg/g)	56.4864	65.157	56.7582	79.3366
B_D (mol^2/KJ^2)	6×10^{-6}	3×10^{-7}	3×10^{-6}	1×10^{-7}
E_D (KJ/mol)	0.28	0.41	0.40	0.71
R^2	0.9219	0.9482	0.9282	0.9346
RMSE	3.0368	10.272	10.0011	17.948

$$\ln K_d = \frac{-\Delta H^\circ}{RT} + \frac{\Delta S^\circ}{R}, \tag{26}$$

$$\Delta G^\circ = -RT \ln K_d, \tag{27}$$

$$K_d = \frac{Q_e}{C_e}, \tag{28}$$

where K_d is the equilibrium constant. ΔG°, ΔH°, and ΔS° are Gibbs free energy, enthalpy, and entropy, respectively. ΔH° and ΔS° are determined from Van't Hoff plots. A favorable adsorption process is the one that shows negative (ΔG°) and increased K_d with the advancement of temperature [81]. ($0 > \Delta H^\circ$) shows the exothermic nature of the CR adsorption, and ($0 < \Delta S^\circ$) shows increased randomness or entropy of the process. Activation energy is determined by the Arrhenius equation:

$$\ln k = \frac{\ln A - E_a}{RT}, \tag{29}$$

where A is the frequency factor. Overall, the reaction comes out to be a physical one.

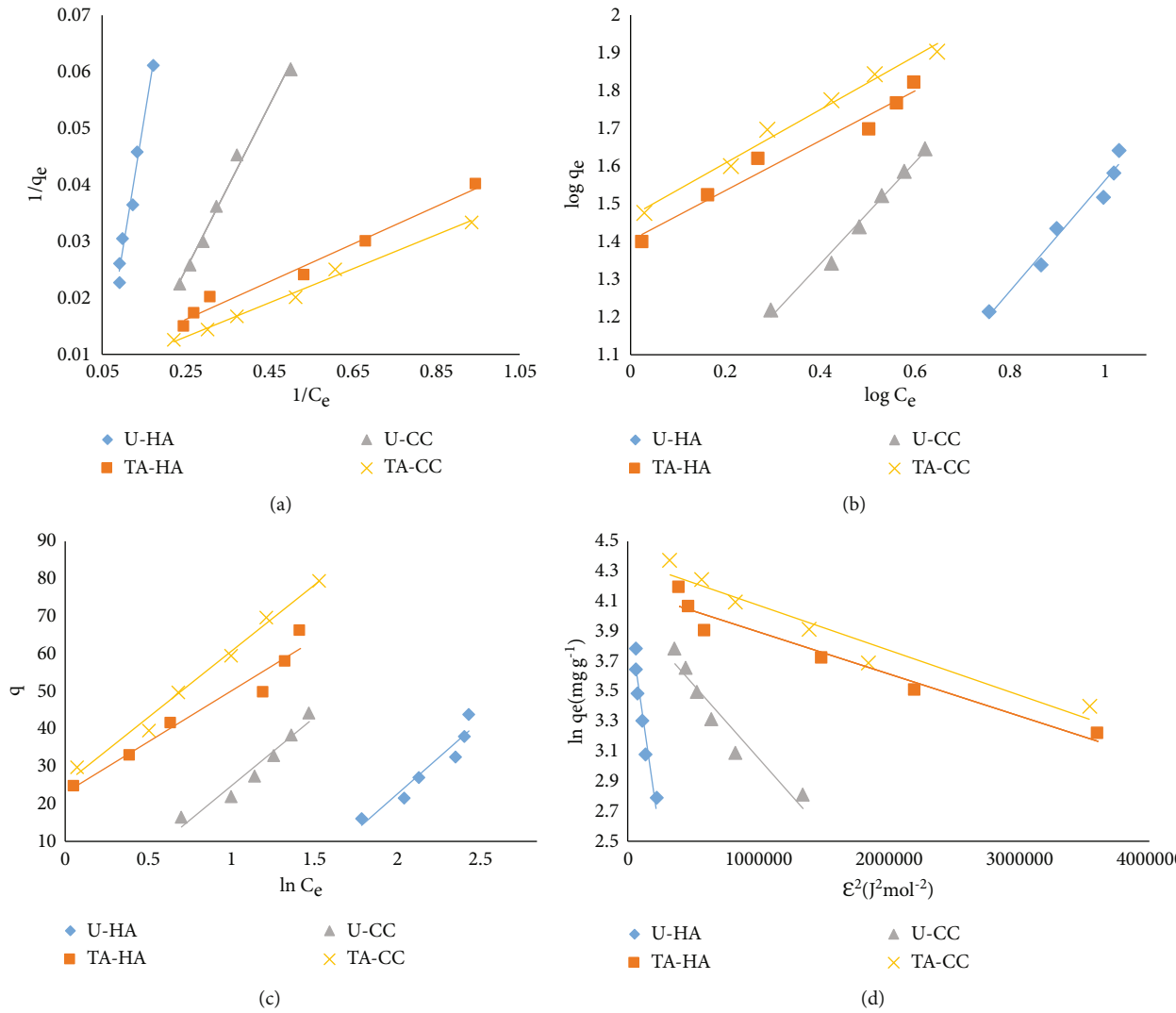

Figure 6: (a) Langmuir (b) Freundlich, (c) Temkin, and (d) D-R isothermal studies for CR dye.

3.12. Adsorption Mechanism. Different functional moieties such as (−COOH), (−SO), ($-NH_2$), and (−OH) are present in the adsorbents that are responsible for the binding of the dye. A basic pH converts these groups into anionic forms (COO^-) and (OH^-) and is unable to adsorb negatively charged dye particles because of interionic repulsion among similar charged entities. Excessive OH^- ions that compete for potential sites hinder the adsorption of anionic dyes at higher pH. For CR, the isoelectronic point is 3.0 and it occurs in negatively charged forms in the pH range of 5.0-10.0. Point of zero charge pH_{pzc} was demonstrated that the adsorbent surface was positive below 6 (U-HA) and 5 (U-CC) and negative above it. Carboxylate ions have pKa 3.0-5.0, below which it dissociates into positively charged species. In an acidic solution, CR dissociates into polar groups (SO_3^-) and adsorbs on positively charged adsorbent [44], inducing electrostatic interactions between the surface and dye [82]. Hydrogen bonding occurs between oxygen (carbonyl and carboxyl) and nitrogen-containing functional groups of CR and adsorbents [82].

The FTIR spectra when observed displayed variations in wavenumbers and peak intensities of the raw and modified dye adsorptions. For example, the peaks of hydroxyl stretching 3737.6 cm^{-1}, 3653.0 cm^{-1}, and 3568.7 cm^{-1} in IR of U-HA adsorbents when reacted with CR (Figure 2(a)) shifted towards 3872 cm^{-1}, 3855 cm^{-1}, and 3752 cm^{-1} for TA-HA with CR (Figure 2(b)). The second adsorbent U-CC when treated with CR was seen to consist of -OH stretch at 3568 cm^{-1} and 3737 cm^{-1} (Figure 2(c)), when TA-CC was treated with CR new peaks displaying hydroxyl groups were observed such as 3904 cm^{-1}, 3841 cm^{-1}, 3631 cm^{-1}, and 3547 cm^{-1} (Figure 2(d)).

Also, peaks corresponding to -C=O groups show a slight shift in wavenumbers, demonstrating the involvement of surface oxygen functionalities in dye removal. Strong electrostatic and chemical binding is the dominant phenomenon in removing CR from an aqueous phase.

The peaks at 2922 cm^{-1}, 2853 cm^{-1}, and 2850 cm^{-1} corresponding towards asymmetric and symmetric sp^3 C-H stretch in U-HA adsorbent (Figure 2(a)) show reduced peaks

Table 4: Thermodynamic parameters for CR dye adsorption.

Adsorbents	T (K)	ΔG° (kJmol^{-1})	K_D	ΔH° (kJmol^{-1})	ΔS° (Jmol^{-1} K^{-1})	E_a (kJmol^{-1})
U-HA	283	-1.3445	1.770619	-48.9993044	180.941278	21.276294
	293	-1.74341	2.045326			
	303	-2.07376	2.277439			
	313	-2.4044	2.518822			
	323	-4.9317	6.651246			
TA-HA	283	-2.14711	2.49026	-56.44781139	214.45573	24.5105564
	293	-2.56614	2.866906			
	303	-3.3066	3.714912			
	313	-4.67482	6.026144			
	323	-5.81927	8.728507			
U-CC	283	-1.41599	1.82523	-25.48959516	101.2978	11.068
	293	-1.82091	2.111433			
	303	-2.15721	2.354134			
	313	-2.7413	2.866906			
	323	-3.16494	3.249012			
TA-CC	283	-2.28265	2.637902	-44.08980004	171.2372	19.1445079
	293	-2.44928	2.732639			
	303	-2.96897	3.249012			
	313	-3.79373	4.295567			
	323	-5.43528	7.565737			

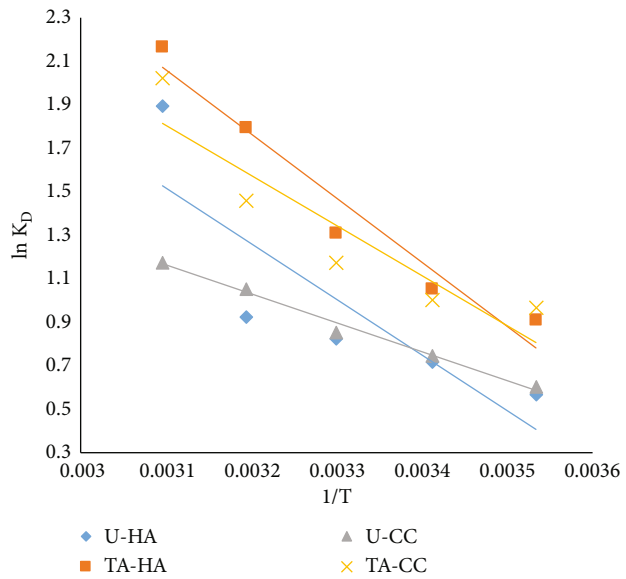

Figure 7: Thermodynamic studies for CR dye.

of 2921 cm^{-1} and 2852 cm^{-1} in modified forms (Figure 2(b)). In the second adsorbent U-CC, alkane C-H at 2850 cm^{-1} (Figure 2(c)) shifted to alkyl C-H stretch at 2923.9 cm^{-1} (Figure 2(d)). This is evident of C-H groups as potential sites contributing to the removal of CR from the water phase via pi-pi interactions. The isothermal studies showed a greater correlation of the Langmuir isotherm than other models leading towards chemisorption.

Strong hydrophobic interactions are the result of size and hydrophilicity of CR dye. Physisorption involving surface adsorption and hydrophobic and pi-pi interactions are observed with the adsorbent surfaces. In addition to these, strong electrostatic interactions along with the chemical binding of the oxygen functionalities are engaged in CR removal from the active sites.

Thus, the adsorption mechanism (Figure 8) is a complex physicochemical procedure [83] involving electrostatic interactions, chemical binding with surface functionalities, and hydrogen bondings. Similar mechanisms were proved by Lafi et al. using coffee waste-activated carbon [52] and Al-Zoubi et al. with jojoba residues [83].

3.13. Comparison with Other Adsorbents. Traditionally used biosorbents pose significant problems towards the adsorption procedure such as slow adsorption kinetics and lesser adsorption capacities. The purification of wastewaters should be efficient and able to neutralize effluents and return purified water and valuable components of production [2, 84]. As mentioned in the following (Table 5), CR was removed from the modified adsorbents in an efficient manner and the adsorbents followed all the aforementioned properties of a good adsorbent. The adsorbents are efficient, inexpensive, and readily available. High adsorption capacities are achieved, and modifying them with more advanced smart materials will enhance them more. Further research is still needed to adopt new pathways for studying their properties and expediency of their functionalization.

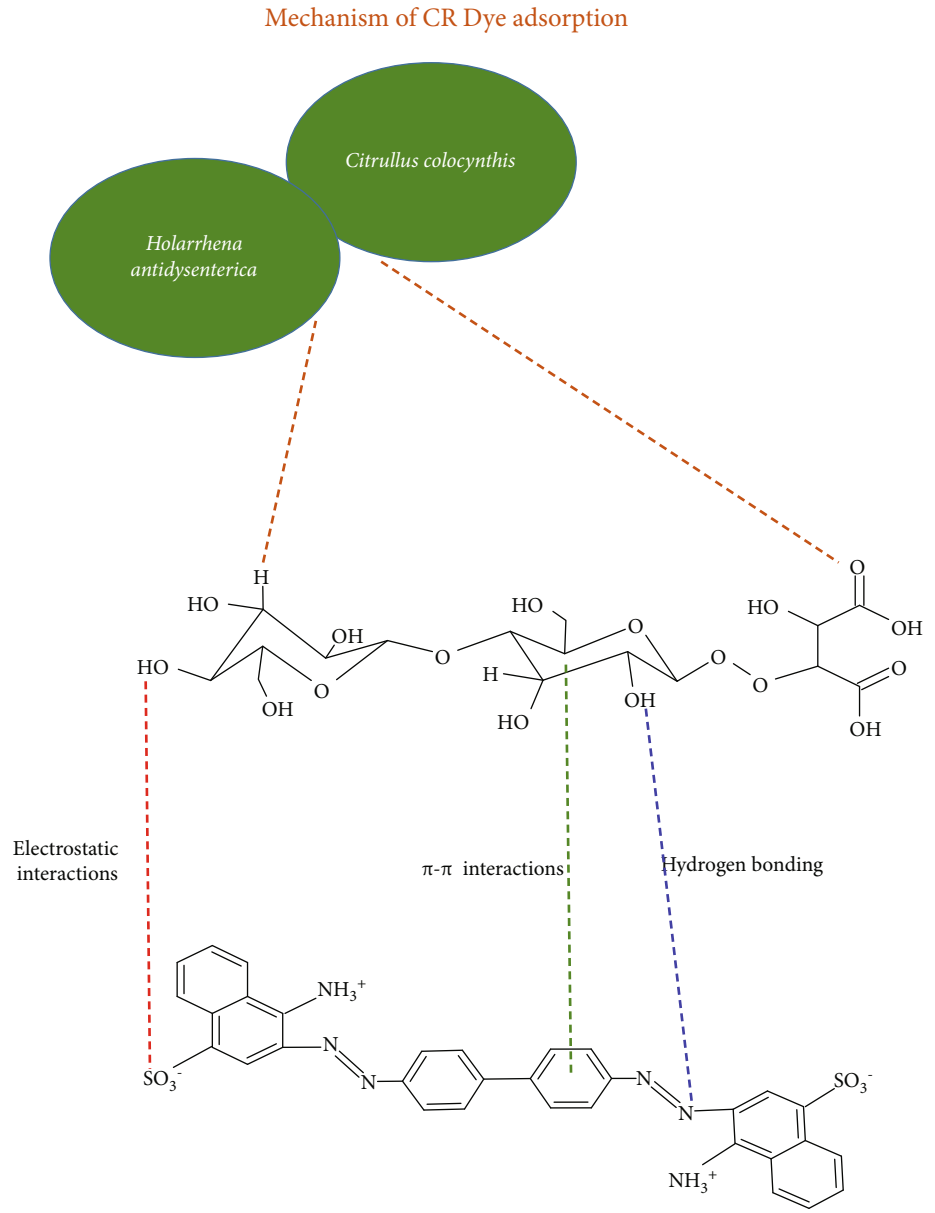

Figure 8: Proposed mechanism of CR dye adsorption.

3.14. Regeneration Study. Regeneration was performed in three consecutive cycles, which yielded about 80%, 88%, 84%, and 90% dye removal for U-HA, TA-HA, U-CC, and TA-CC, respectively.

3.15. Novelty of the Procedure. Within the scope of the authors' exhaustive search, *Holarrhena antidysenterica* and *Citrullus colocynthis* are unreported for the adsorption of Congo red dye contributing towards the novelty of the current research. The ability of modified adsorbents for the efficient and low-cost removal of Congo red dye contaminant from wastewaters has been evaluated, and mechanistic study of adsorption was fully comprehended.

3.16. Research Limitations/Implications. Usage of these adsorbents for metal sequestration, organic pollutant elimi-

Table 5: Estimation of Q_{max} between previous and experimented adsorbents.

Adsorbents	Q_{max} (mg g^{-1})	Reference
Wheat straw	71.2	[72]
Trametes versicolor	51.81	[85]
Jojoba seeds	58.82	[83]
Green coffee residues	20.04	[86]
Pinus pinaster bark	3.92	[87]
U-HA	60.61	This study
TA-HA	128.21	This study
U-CC	87.71	This study
TA-CC	131.57	This study

nation, activated carbon manufacturing, and nanoadsorbent functioning in advanced wastewater treatments is the further and future investigation underway.

4. Conclusions

Thus, it is concluded that adsorbents U-HA and U-CC are cheap and environmentally friendly possessing high dye removal properties. Their possession of higher oxygen-containing functionalities after the treatment with tartaric acid makes them the most promising candidates. FTIR and SEM studies confirm the presence of -COOH and -OH groups that bind CR with hydrophobic, pi-pi, chemical, and electrostatic interactions. Exterior surfaces pose ample binding surfaces for dye binding followed by the transfer of dye within the interior as evident from Boyd's and Webber-Morris plots. The Langmuir model gave Q_{max} 128 ($mg\,g^{-1}$) for TA-HA and 131 ($mg\,g^{-1}$) for TA-CC with dye removal. Both treated and untreated adsorbents were in correspondence towards the pseudo-second-order kinetic model. Thermodynamics proved the procedure exothermic and spontaneous along with increasing randomness in the system.

Data Availability

All data related to this work is presented in the results section along with references.

Conflicts of Interest

Regarding the publication of this article, we have no potential conflict of interest.

Acknowledgments

The authors are thankful to the home department for funding this work.

References

[1] I. Ali, T. A. Khan, and I. Hussain, "Treatment and remediation methods for arsenic removal from the ground water," *International journal of environmental engineering*, vol. 3, no. 1, pp. 48–71, 2011.

[2] I. Ali, T. Kon'kova, V. Kasianov et al., "Preparation and characterization of nano-structured modified montmorillonite for dioxidine antibacterial drug removal in water," *Journal of Molecular Liquids*, vol. 331, article 115770, 2021.

[3] A. A. Basheer, "Chemical chiral pollution: impact on the society and science and need of the regulations in the 21stcentury," *Chirality*, vol. 30, no. 4, pp. 402–406, 2018.

[4] Z. A. ALOthman, A. Y. Badjah, and I. Ali, "Facile synthesis and characterization of multi walled carbon nanotubes for fast and effective removal of 4-tert-octylphenol endocrine disruptor in water," *Journal of Molecular Liquids*, vol. 275, pp. 41–48, 2019.

[5] F. Saputra, C.-H. Yen, C.-Y. Hsieh et al., "Toxicity effects of the environmental hormone 4-tert-octylphenol in zebrafish (Danio rerio)," *International Journal of Marine Science*, vol. 6, 2016.

[6] A. A. Basheer and I. Ali, "Stereoselective uptake and degradation of (±)-o, p-DDD pesticide stereomers in water-sediment system," *Chirality*, vol. 30, no. 9, pp. 1088–1095, 2018.

[7] G. Sharma, V. K. Gupta, S. Agarwal, A. Kumar, S. Thakur, and D. Pathania, "Fabrication and characterization of nanoparticles: ion exchange behavior and photocatalytic activity against malachite green," *Journal of Molecular Liquids*, vol. 219, pp. 1137–1143, 2016.

[8] R. Shokoohi, M. Salari, R. Safari, H. Zolghadr Nasab, and S. Shanehsaz, "Modelling and optimisation of catalytic ozonation process assisted by ZrO_2-pumice/H_2O_2in the degradation of rhodamine B dye from aqueous environment," *International Journal of Environmental Analytical Chemistry*, vol. 101, no. 15, pp. 2629–2653, 2021.

[9] R. H. Thabet, M. K. Fouad, I. Ali, S. A. El Sherbiney, and M. A. Tony, "Magnetite-based nanoparticles as an efficient hybrid heterogeneous adsorption/oxidation process for reactive textile dye removal from wastewater matrix," *International Journal of Environmental Analytical Chemistry*, pp. 1–23, 2021.

[10] R. Tayebee, E. Esmaeili, B. Maleki, A. Khoshniat, M. Chahkandi, and N. Mollania, "Photodegradation of methylene blue and some emerging pharmaceutical micropollutants with an aqueous suspension of WZnO-NH_2@ $H_3PW_{12}O_{40}$ nanocomposite," *Journal of Molecular Liquids*, vol. 317, article 113928, 2020.

[11] H. Yang, J. Zhang, Y. Liu et al., "Rapid removal of anionic dye from water by poly (ionic liquid)-modified magnetic nanoparticles," *Journal of Molecular Liquids*, vol. 284, pp. 383–392, 2019.

[12] M. Fatima, R. Farooq, R. W. Lindström, and M. Saeed, "A review on biocatalytic decomposition of azo dyes and electrons recovery," *Journal of Molecular Liquids*, vol. 246, pp. 275–281, 2017.

[13] C. R. Marcelo, G. A. Puiatti, M. A. Nascimento, A. F. Oliveira, and R. P. Lopes, "Degradation of the reactive blue 4 dye in aqueous solution using zero-valent copper nanoparticles," *Journal of Nanomaterials*, vol. 2018, Article ID 4642038, 9 pages, 2018.

[14] I. Ali, S. Afshinb, Y. Poureshgh et al., "Green preparation of activated carbon from pomegranate peel coated with zero-valent iron nanoparticles (nZVI) and isotherm and kinetic studies of amoxicillin removal in water," *Environmental Science and Pollution Research*, vol. 27, no. 29, pp. 36732–36743, 2020.

[15] I. Burakova, A. Burakov, A. Tkachev et al., "Kinetics of the adsorption of scandium and cerium ions in sulfuric acid solutions on a nanomodified activated carbon," *Journal of Molecular Liquids*, vol. 253, pp. 277–283, 2018.

[16] A. Yazidi, L. Sellaoui, G. L. Dotto, A. Bonilla-Petriciolet, A. C. Fröhlich, and A. B. Lamine, "Monolayer and multilayer adsorption of pharmaceuticals on activated carbon: application of advanced statistical physics models," *Journal of Molecular Liquids*, vol. 283, pp. 276–286, 2019.

[17] A. Stavrinou, C. Aggelopoulos, and C. Tsakiroglou, "Exploring the adsorption mechanisms of cationic and anionic dyes onto agricultural waste peels of banana, cucumber and potato: adsorption kinetics and equilibrium isotherms as a tool," *Journal of Environmental Chemical Engineering*, vol. 6, no. 6, pp. 6958–6970, 2018.

[18] I. Ali, O. M. Alharbi, Z. A. ALOthman, A. Alwarthan, and A. M. al-Mohaimeed, "Preparation of a carboxymethylcellulose-iron composite for uptake of

atorvastatin in water," *International Journal of Biological Macromolecules*, vol. 132, pp. 244–253, 2019.

[19] I. Ali, O. M. Alharbi, Z. A. Alothman, and A. Y. Badjah, "Kinetics, thermodynamics, and modeling of amido black dye photodegradation in water using Co/TiO_2 nanoparticles," *Photochemistry and Photobiology*, vol. 94, no. 5, pp. 935–941, 2018.

[20] P. Rath, S. Behera, B. Priyadarshini et al., "Influence of Mg doping on ZnO NPs for enhanced adsorption activity of Congo red dye," *Applied Surface Science*, vol. 491, pp. 256–266, 2019.

[21] B. Priyadarshini, T. Patra, and T. R. Sahoo, "An efficient and comparative adsorption of Congo red and trypan blue dyes on MgO nanoparticles: kinetics, thermodynamics and isotherm studies," *Journal of Magnesium and Alloys*, vol. 9, no. 2, pp. 478–488, 2021.

[22] Z. Wu, X. Yuan, H. Zhong et al., "Highly efficient adsorption of Congo red in single and binary water with cationic dyes by reduced graphene oxide decorated NH2-MIL-68 (Al)," *Journal of Molecular Liquids*, vol. 247, pp. 215–229, 2017.

[23] K. Elwakeel, A. Elgarahy, G. Elshoubaky, and S. Mohammad, "Microwave assist sorption of crystal violet and Congo red dyes onto amphoteric sorbent based on upcycled sepia shells," *Journal of Environmental Health Science and Engineering*, vol. 18, no. 1, pp. 35–50, 2020.

[24] M. R. Abukhadra, A. Adlii, and B. M. Bakry, "Green fabrication of bentonite/ oxide composite (BE/) of enhanced adsorption and advanced oxidation removal of Congo red dye and Cr (VI) from water," *International Journal of Biological Macromolecules*, vol. 126, pp. 402–413, 2019.

[25] A. A. Alqadami, M. Naushad, M. A. Abdalla et al., "Efficient removal of toxic metal ions from wastewater using a recyclable nanocomposite: a study of adsorption parameters and interaction mechanism," *Journal of Cleaner Production*, vol. 156, pp. 426–436, 2017.

[26] F. K. Liew, S. Hamdan, M. Rahman et al., "Synthesis and characterization of cellulose from green bamboo by chemical treatment with mechanical process," *Journal of Chemistry*, vol. 2015, Article ID 212158, 6 pages, 2015.

[27] G. Enaime, A. Baçaoui, A. Yaacoubi, and M. Lübken, "Biochar for wastewater treatment—conversion technologies and applications," *Applied Sciences*, vol. 10, no. 10, p. 3492, 2020.

[28] Y. Chen, Y. Zhu, Z. Wang et al., "Application studies of activated carbon derived from rice husks produced by chemical-thermal process—a review," *Advances in Colloid and Interface Science*, vol. 163, no. 1, pp. 39–52, 2011.

[29] S. S. Pillai, M. D. Mullassery, N. B. Fernandez, N. Girija, P. Geetha, and M. Koshy, "Biosorption of Cr(VI) from aqueous solution by chemically modified potato starch: equilibrium and kinetic studies," *Ecotoxicology and Environmental Safety*, vol. 92, pp. 199–205, 2013.

[30] A. Ş. Yargıç, R. Y. Şahin, N. Özbay, and E. Önal, "Assessment of toxic copper (II) biosorption from aqueous solution by chemically-treated tomato waste," *Journal of Cleaner Production*, vol. 88, pp. 152–159, 2015.

[31] L. W. Low, T. T. Teng, N. Morad, and B. Azahari, "Studies on the adsorption of methylene blue dye from aqueous solution onto low-cost tartaric acid treated bagasse," *APCBEE Procedia*, vol. 1, pp. 103–109, 2012.

[32] B. C. S. Ferreira, F. S. Teodoro, A. B. Mageste, L. F. Gil, R. P. de Freitas, and L. V. A. Gurgel, "Application of a new carboxylate-functionalized sugarcane bagasse for adsorptive removal of crystal violet from aqueous solution: kinetic, equilibrium and thermodynamic studies," *Industrial Crops and Products*, vol. 65, pp. 521–534, 2015.

[33] N. Mojoudi, N. Mirghaffari, M. Soleimani, H. Shariatmadari, C. Belver, and J. Bedia, "Phenol adsorption on high microporous activated carbons prepared from oily sludge: equilibrium, kinetic and thermodynamic studies," *Scientific Reports*, vol. 9, no. 1, pp. 1–12, 2019.

[34] A. Daochalermwong, N. Chanka, K. Songsrirote, P. Dittanet, C. Niamnuy, and A. Seubsai, "Removal of heavy metal ions using modified celluloses prepared from pineapple leaf fiber," *ACS Omega*, vol. 5, no. 10, pp. 5285–5296, 2020.

[35] A. Mittal, R. Katahira, M. E. Himmel, and D. K. Johnson, "Effects of alkaline or liquid-ammonia treatment on crystalline cellulose: changes in crystalline structure and effects on enzymatic digestibility," *Biotechnology for Biofuels*, vol. 4, no. 1, pp. 1–16, 2011.

[36] T. Mahmud, "Biosorption of Auramine O and Drimarene dyes from aqueous solutions using seed powder of *Diospyros lotus*," *International Journal of Environment and Sustainability*, vol. 6, no. 3, 2018.

[37] S. Basharat, R. Rehman, T. Mahmud, S. Basharat, and L. Mitu, "Tartaric acid-modified *Holarrhena antidysenterica* and *Citrullus colocynthis* biowaste for efficient eradication of crystal violet dye from water," *Journal of Chemistry*, vol. 2020, Article ID 8862167, 18 pages, 2020.

[38] D. Chowdhuri, R. Nakul, G. P. Jeppu, and P. Vairavel, "Process optimization, isotherm, kinetics, and thermodynamics studies for removal of remazol brilliant blue-R dye from contaminated water using adsorption on guava leaf powder," *Desalination and Water Treatment*, vol. 185, pp. 318–343, 2020.

[39] P. Vairavel, N. Rampal, and G. Jeppu, "Adsorption of toxic Congo red dye from aqueous solution using untreated coffee husks: kinetics, equilibrium, thermodynamics and desorption study," *International Journal of Environmental Analytical Chemistry*, pp. 1–20, 2021.

[40] A. N. Alene, G. Y. Abate, and A. T. Habte, "Bioadsorption of basic blue dye from aqueous solution onto raw and modified waste ash as economical alternative bioadsorbent," *Journal of Chemistry*, vol. 2020, Article ID 8746035, 11 pages, 2020.

[41] H. P. Boehm, "Surface oxides on carbon and their analysis: a critical assessment," *Carbon*, vol. 40, no. 2, pp. 145–149, 2002.

[42] M. Moradi, M. Hosseini Sabzevari, F. Marahel, and A. Shameli, "Removal of reactive green KE-4BD and Congo red dyes in textile effluent by natural clinoptilolite particles on a biosorbent as a cheap and efficient adsorbent: experimental design and optimisation," *International Journal of Environmental Analytical Chemistry*, pp. 1–19, 2021.

[43] R. Nodehi, H. Shayesteh, and A. R. Kelishami, "Enhanced adsorption of Congo red using cationic surfactant functionalized zeolite particles," *Microchemical Journal*, vol. 153, article 104281, 2020.

[44] R. M. Kulkarni, R. Vaidya, S. Srinivas, S. Anand, and B. Narayana, "Application of water hyacinth root powder for Congo red dye removal in batch and continuous packed bed operation," *Nanotechnology for Environmental Engineering*, vol. 6, no. 2, pp. 1–11, 2021.

[45] M. Naushad, G. Sharma, A. Kumar et al., "Efficient removal of toxic phosphate anions from aqueous environment using pectin based quaternary amino anion exchanger," *International Journal of Biological Macromolecules*, vol. 106, pp. 1–10, 2018.

[46] A. M. Abbas, F. H. Abdulrazzak, and T. Himdan, "Kinetic study of adsorption of azo dye from aqueous solutions by zeolite and modified synthetic zeolite," *Journal of Materials and Environmental Science*, vol. 9, no. 9, pp. 2652–2659, 2018.

[47] I. Ali, O. M. Alharbi, Z. A. ALOthman, A. M. al-Mohaimeed, and A. Alwarthan, "Modeling of fenuron pesticide adsorption on CNTs for mechanistic insight and removal in water," *Environmental Research*, vol. 170, pp. 389–397, 2019.

[48] M. Foroughi-Dahr, H. Abolghasemi, M. Esmaili, A. Shojamoradi, and H. Fatoorehchi, "Adsorption characteristics of Congo red from aqueous solution onto tea waste," *Chemical Engineering Communications*, vol. 202, no. 2, pp. 181–193, 2015.

[49] A. Chham, E. Khouya, M. Oumam et al., "The use of insoluble mater of Moroccan oil shale for removal of dyes from aqueous solution," *Chemistry International*, vol. 4, no. 1, pp. 67–77, 2018.

[50] A. Gouza, K. Fanidi, S. Saoiabi, A. Laghzizil, and A. Saoiabi, "Effect of heat treatment on the surface properties of selected bituminous shale for cationic dye sorption," *Desalination and Water Treatment*, vol. 66, pp. 274–280, 2017.

[51] M. El Haddad, R. Slimani, R. Mamouni, S. ElAntri, and S. Lazar, "Removal of two textile dyes from aqueous solutions onto calcined bones," *Journal of the Association of Arab Universities for Basic and Applied Sciences*, vol. 14, no. 1, pp. 51–59, 2013.

[52] R. Lafi, I. Montasser, and A. Hafiane, "Adsorption of Congo red dye from aqueous solutions by prepared activated carbon with oxygen-containing functional groups and its regeneration," *Adsorption Science & Technology*, vol. 37, no. 1-2, pp. 160–181, 2019.

[53] Z. L. Yaneva and N. V. Georgieva, "Insights into Congo red adsorption on agro-industrial materials-spectral, equilibrium, kinetic, thermodynamic, dynamic and desorption studies. A Review," *International Review of Chemical Engineering*, vol. 4, no. 2, pp. 127–146, 2012.

[54] H. Shayesteh, A. Rahbar-Kelishami, and R. Norouzbeigi, "Evaluation of natural and cationic surfactant modified pumice for Congo red removal in batch mode: kinetic, equilibrium, and thermodynamic studies," *Journal of Molecular Liquids*, vol. 221, pp. 1–11, 2016.

[55] S. W. Won, K. Vijayaraghavan, J. Mao, S. Kim, and Y.-S. Yun, "Reinforcement of carboxyl groups in the surface of *Corynebacterium glutamicum* biomass for effective removal of basic dyes," *Bioresource Technology*, vol. 100, no. 24, pp. 6301–6306, 2009.

[56] S. Coruh, S. Elevli, and G. Doğan, "Optimization study of adsorption of crystal violet and Congo red onto sepiolite and clinoptilolite," *Global NEST Journal*, vol. 19, 2019.

[57] S. J. Santosa, "Adsorption of Congo Red Dye on HDTMA Surfactant-Modified Zeolite A Synthesized from Fly Ash," in *Defect and Diffusion Forum*, Trans Tech Publications Ltd, 2018.

[58] J. Song, W. Zou, Y. Bian, F. Su, and R. Han, "Adsorption characteristics of methylene blue by peanut husk in batch and column modes," *Desalination*, vol. 265, no. 1-3, pp. 119–125, 2011.

[59] N. El Messaoudi, M. El Khomri, Z. G. Chegini et al., "Dye removal from aqueous solution using nanocomposite synthesized from oxalic acid-modified agricultural solid waste and $ZnFe_2O_4$ nanoparticles," *Nanotechnology for Environmental Engineering*, vol. 7, no. 1, pp. 1–15, 2021.

[60] C. Cheung, J. Porter, and G. McKay, "Sorption kinetic analysis for the removal of cadmium ions from effluents using bone char," *Water Research*, vol. 35, no. 3, pp. 605–612, 2001.

[61] V. Verma and A. Mishra, "Kinetic and isotherm modeling of adsorption of dyes onto rice husk carbon," *Global NEST Journal*, vol. 12, no. 2, pp. 190–196, 2019.

[62] M. A. Islam, A. Benhouria, M. Asif, and B. Hameed, "Methylene blue adsorption on factory-rejected tea activated carbon prepared by conjunction of hydrothermal carbonization and sodium hydroxide activation processes," *Journal of the Taiwan Institute of Chemical Engineers*, vol. 52, pp. 57–64, 2015.

[63] K. Y. Chong, C. H. Chia, S. Zakaria, and M. S. Sajab, "Vaterite calcium carbonate for the adsorption of Congo red from aqueous solutions," *Journal of Environmental Chemical Engineering*, vol. 2, no. 4, pp. 2156–2161, 2014.

[64] C. A. Igwegbe, O. D. Onukwuli, K. K. Onyechi, and S. Ahmadi, "Equilibrium and kinetics analysis on vat yellow 4 uptake from aqueous environment by modified rubber seed shells: nonlinear modelling," *Journal of Materials and Environmental Science*, vol. 11, no. 9, pp. 1424–1444, 2020.

[65] K. Tan and B. Hameed, "Insight into the adsorption kinetics models for the removal of contaminants from aqueous solutions," *Journal of the Taiwan Institute of Chemical Engineers*, vol. 74, pp. 25–48, 2017.

[66] W. J. Weber and J. C. Morris, "Kinetics of adsorption on carbon from solution," *Journal of the Sanitary Engineering Division*, vol. 89, no. 2, pp. 31–59, 1963.

[67] A. Kumar, S. Kumar, and S. Kumar, "Adsorption of resorcinol and catechol on granular activated carbon: equilibrium and kinetics," *Carbon*, vol. 41, no. 15, pp. 3015–3025, 2003.

[68] A. Chaib, N. Boukhalfa, and A. Boudjemaa, "Congo red removal using Fesdis soil: kinetic, equilibrium and thermodynamic studies," *International Journal of Environmental Analytical Chemistry*, pp. 1–21, 2021.

[69] M. B. Amran and M. A. Zulfikar, "Removal of Congo red dye by adsorption onto phyrophyllite," *International Journal of Environmental Studies*, vol. 67, no. 6, pp. 911–921, 2010.

[70] R. Abdul, M. Tariq, A. Muhammad, R. Rabia, and B. Sumaira, "Usage of fruit-fibers of *Luffa cylindrica* for the sorptive removal of direct blue 15 dye from water," *Desalination and Water Treatment*, vol. 120, pp. 350–360, 2018.

[71] R. Fiaz, M. Hafeez, and R. Mahmood, "Removal of brilliant green (BG) from aqueous solution by using low cost biomass *Salix alba* leaves (SAL): thermodynamic and kinetic studies," *Journal of Water Reuse and Desalination*, vol. 10, no. 1, pp. 70–81, 2020.

[72] R. Zhang, J. Zhang, X. Zhang, C. Dou, and R. Han, "Adsorption of Congo red from aqueous solutions using cationic surfactant modified wheat straw in batch mode: kinetic and equilibrium study," *Journal of the Taiwan Institute of Chemical Engineers*, vol. 45, no. 5, pp. 2578–2583, 2014.

[73] I. Langmuir, "The adsorption of gases on plane surfaces of glass, mica and platinum," *Journal of the American Chemical Society*, vol. 40, no. 9, pp. 1361–1403, 1918.

[74] A. Benmessaoud, D. Nibou, E. H. Mekatel, and S. Amokrane, "A comparative study of the linear and non-linear methods for determination of the optimum equilibrium isotherm for adsorption of Pb^{2+} ions onto Algerian treated clay," *Iranian Journal of Chemistry and Chemical Engineering (IJCCE)*, vol. 39, no. 4, pp. 153–171, 2020.

[75] C. Yahiaoui, M. Kameche, C. Innocent, and A. Khenifi, "Conception of yeast microbial desalination cell: applications to dye wastewater treatment and lead removal," *Chemical Engineering Communications*, vol. 208, no. 3, pp. 364–375, 2021.

[76] I. Ali, A. E. Burakov, A. V. Melezhik et al., "Removal of copper (II) and zinc (II) ions in water on a newly synthesized polyhydroquinone/graphene nanocomposite material: kinetics, thermodynamics and mechanism," *Chemistry Select*, vol. 4, no. 43, pp. 12708–12718, 2019.

[77] M. A. E. Barakat, R. Kumar, M. K. Seliem et al., "Exfoliated clay decorated with magnetic iron nanoparticles for crystal violet adsorption: modeling and physicochemical interpretation," *Nanomaterials*, vol. 10, no. 8, p. 1454, 2020.

[78] M. H. Jnr and A. I. Spiff, "Equilibrium sorption study of Al^{3+}, Co^{2+} and Ag^{+} in aqueous solutions by fluted pumpkin (*Telfairia occidentalis* HOOK f) waste biomass," *Acta Chimica Slovenica*, vol. 52, pp. 174–181, 2005.

[79] O. Celebi, Ç. Üzüm, T. Shahwan, and H. N. Erten, "A radiotracer study of the adsorption behavior of aqueous Ba^{2+} ions on nanoparticles of zero-valent iron," *Journal of Hazardous Materials*, vol. 148, no. 3, pp. 761–767, 2007.

[80] J. O. Eniola, R. Kumar, A. A. Al-Rashdi, M. O. Ansari, and M. A. Barakat, "Fabrication of novel Al $(OH)_3$/CuMnAl-layered double hydroxide for detoxification of organic contaminants from aqueous solution," *ACS Omega*, vol. 4, no. 19, pp. 18268–18278, 2019.

[81] J. O. Ighalo and A. G. Adeniyi, "Adsorption of pollutants by plant bark derived adsorbents: an empirical review," *Journal of Water Process Engineering*, vol. 35, article 101228, 2020.

[82] G. Sriram, U. Uthappa, D. Losic, M. Kigga, H.-Y. Jung, and M. D. Kurkuri, "Mg–Al-layered double hydroxide (LDH) modified diatoms for highly efficient removal of Congo red from aqueous solution," *Applied Sciences*, vol. 10, no. 7, p. 2285, 2020.

[83] H. Al-Zoubi, M. Zubair, M. S. Manzar et al., "Comparative adsorption of anionic dyes (eriochrome black t and Congo red) onto jojoba residues: isotherm, kinetics and thermodynamic studies," *Arabian Journal for Science and Engineering*, vol. 45, no. 9, pp. 7275–7287, 2020.

[84] I. Ali, A. V. Babkin, I. V. Burakova et al., "Fast removal of samarium ions in water on highly efficient nanocomposite based graphene oxide modified with polyhydroquinone: isotherms, kinetics, thermodynamics and desorption," *Journal of Molecular Liquids*, vol. 329, article 115584, 2021.

[85] A. Binupriya, M. Sathishkumar, K. Swaminathan, C. Kuz, and S. Yun, "Comparative studies on removal of Congo red by native and modified mycelial pellets of *Trametes versicolor* in various reactor modes," *Bioresource Technology*, vol. 99, no. 5, pp. 1080–1088, 2008.

[86] M. S. Manzar, M. Zubair, N. A. Khan et al., "Adsorption behaviour of green coffee residues for decolourization of hazardous Congo red and eriochrome black T dyes from aqueous solutions," *International Journal of Environmental Analytical Chemistry*, pp. 1–17, 2020.

[87] K. Litefti, M. S. Freire, M. Stitou, and J. González-Álvarez, "Adsorption of an anionic dye (Congo red) from aqueous solutions by pine bark," *Scientific Reports*, vol. 9, no. 1, pp. 1–11, 2019.